Proceedings of ASME Turbo Expo 2003
Power for Land, Sea, and Air
June 16-19, 2003, Atlanta, Georgia, USA

GT2003-38553

CONJUGATE HEAT TRANSFER EFFECTS ON A REALISTIC FILM-COOLED TURBINE VANE

James D. Heidmann
NASA Glenn Research Center
Cleveland, OH

Alain J. Kassab
Eduardo A. Divo
Franklin Rodriguez
University of Central Florida
Orlando, FL

Erlendur Steinthorsson
A&E Consulting
Westlake, OH

ABSTRACT

A conjugate heat transfer solver has been developed and applied to a realistic film-cooled turbine vane for a variety of blade materials. The solver used for the fluid convection part of the problem is the Glenn-HT general multiblock heat transfer code. The solid conduction module is based on the Boundary Element Method (BEM), and is coupled directly to the flow solver. A chief advantage of the BEM method is that no volumetric grid is required inside the solid – only the surface grid is needed. Since a surface grid is readily available from the fluid side of the problem, no additional gridding is required. This eliminates one of the most time consuming elements of the computation for complex geometries. Two conjugate solution examples are presented - a high thermal conductivity Inconel nickel-based alloy vane case and a low thermal conductivity silicon nitride ceramic vane case. The solutions from the conjugate analyses are compared with an adiabatic wall convection solution. It is found that the conjugate heat transfer cases generally have a lower outer wall temperature due to thermal conduction from the outer wall to the plenum. However, some locations of increased temperature are seen in the higher thermal conductivity Inconel vane case. This is a result of the fact that film cooling is a two-temperature problem, which causes the direction of heat flux at the wall to change over the outer surface. Three-dimensional heat conduction in the solid allows for conduction heat transfer along the vane wall in addition to conduction from outer to inner wall. These effects indicate that the conjugate heat transfer in a complicated geometry such as a film-cooled vane is not governed by simple one-dimensional conduction from the vane surface to the plenum surface, especially when the effects of coolant injection are included.

NOMENCLATURE

c_p	specific heat at constant pressure
h	heat transfer coefficient
k	thermal conductivity
q”	wall heat flux
Pr	Prandtl number
Pr_t	turbulent Prandtl number
s	streamwise distance from leading edge
St	Stanton number
T	temperature
V	velocity
y^+	dimensionless grid spacing
ρ	fluid density
h	film effectiveness

Subscripts

aw	adiabatic wall conditions
c	plenum supply conditions
in	freestream inlet conditions
o	stagnation conditions
s	solid
w	wall conditions

INTRODUCTION

In order to improve gas turbine engine thrust-to-weight ratio and specific fuel consumption, combustor exit temperatures must be increased and turbine cooling flow rates reduced compared to present levels. Compressor discharge temperatures are also increasing because of higher pressure ratio cycles, which increases the temperature of the cooling air available for turbine cooling. All of these constraints combine to make thermal management of advanced turbines very difficult. It is imperative, therefore, that analysis tools become available which can more accurately predict the thermal environment of turbines in the engine environment, and do so in a reasonable time.

The traditional method for analyzing the detailed heat transfer on a turbine blade is to first obtain a fluid-side convection solution using either isothermal or constant heat flux conditions at the blade surface. This effectively decouples the fluid solution from the thermal conduction inside the blade material. For a one-temperature external flow problem (one without film cooling), the external flow solution is used to compute a heat transfer coefficient distribution around the blade. For a two-temperature problem (one with film cooling), a second external flow solution is obtained using a different wall boundary condition. The two solutions are then used to compute the heat transfer coefficient and film cooling effectiveness distributions around the blade. If required, this information is used as a boundary condition to a thermal conduction solver such as ANSYS™, which is used to solve for the solid temperature distribution. In this procedure, is implicitly assumed that the wall thermal boundary condition does not affect the computed heat transfer coefficient and film effectiveness distributions. This is generally a fair assumption, as Kays and Crawford [1] suggest a difference of about 4 percent between the heat transfer coefficients for a turbulent flat plate flow with isothermal and constant heat flux wall boundary conditions. However for cases with large gradients in the wall thermal conditions, such as might be found near film cooling holes on a turbine blade, the local differences could be much greater. Of course the entire process (fluid solution, heat transfer coefficient computation, solid solution, wall boundary condition) could be iterated until the coupled thermal problem is converged, but this is less efficient than a fully coupled thermal analysis tool.

Several researchers have investigated coupled conjugate heat transfer analysis of turbine systems. Bohn et al. [2-5] have published several papers describing their Conjugate Calculation Technique (CCT) as applied to gas turbine blades and vanes. Takahashi et al. [6] performed a conjugate analysis of a turbine blade with tip cooling holes, internal cooling, and rotation. Han et al. [7] computed the thermal field for internally cooled turbine vanes using hybrid unstructured grids in the fluid and solid. Rigby and Lepicovsky [8] extended the Glenn-HT convective heat transfer code to solve conjugate heat transfer problems by using a grid inside the solid and setting the velocities there to zero. There have also been several papers describing conjugate heat transfer for other parts of the gas turbine engine, including secondary air systems [9-11] and combustor liner [12]. All these analyses required meshing the solid volume in order to solve the conduction part of the problem.

Li and Kassab [13, 14] and Ye et al. [15] pursued a different method of coupling the fluid and solid thermal problems. The basis for their technique is the Boundary Element Method (BEM) for solution of the solid conduction problem. Since thermal conduction in a solid is governed by the Laplace equation for temperature, it may be solved using only boundary discretization. BEM takes advantage of this fact and does not require meshing of the solid volume. Kassab et al. [16] reported on the coupling of the BEM method with the Glenn-HT code, and showed the importance of including the conjugate heat transfer effects in the thermal solution of a realistic film-cooled turbine vane. The present study applies the coupled Glenn-HT-BEM code to the three-dimensional film-cooled turbine vane of Heidmann et al. [17]. Two different thermal conductivity materials are considered, using representative thermal conductivities for metal and ceramic vanes. Comparisons are also made to an adiabatic wall boundary condition convection analysis for the same geometry.

VANE GEOMETRY AND NUMERICAL GRID

The turbine vane of this study is based on a Honeywell film-cooled engine design. The geometry is modified for use in a planned NASA Glenn Research Center linear cascade heat transfer experiment. The vane profile is constant in the radial direction, and is based on the engine blade midspan profile, but all the film-cooling hole and plenum geometric details are retained. The geometry of this test vane is scaled up by a factor of 2.943 to allow matching of engine Mach number (0.876) and exit Reynolds number (2.9×10^6 based on true chord) with atmospheric inlet conditions. As shown in Figure 1, the vane has two plena which feed 12 rows of film cooling holes: 4 rows of shaped holes with expanded exits on the pressure side, 6 staggered rows of compound-angled round holes in the showerhead region, and 2 aligned rows of round holes on the suction side. Additional details of the vane geometry are available in Heidmann et al. [17].

A structured multiblock grid is adopted to model this complex geometry. The grid is generated using GridPro™ [18], which produces a body-fitted multiblock grid with hexahedral cells. Since the test vane is of constant radial cross section, only one spanwise pitch of the film cooling hole pattern is discretized, with periodicity enforced at each end. This simplification assumes no endwall effects, but retains the three-dimensionality of the film cooling holes and greatly reduces the

number of grid points required to model the vane. The resultant grid is composed of 140 blocks and 1.2 million computational cells. Algebraic clustering was used to provide a y^+ value of less than 1.0 at the first cell from the wall at all locations. Several calculations were performed for smaller wall spacings, and it was found that further reductions produced little change in the solution. The grid consists of 20 cells across both the inlet and outlet boundaries, 60 cells across the periodic boundary, over 200 cells around the vane, and 44 cells from the vane to the periodic boundary. These values are consistent with good computational practice. A blade-to-blade view of the computational grid is shown in Figure 2.

Figure 3 shows the grid in the leading edge region of the vane. The faithful discretization of the shaped holes should be noted, as well as the ability of the multiblock grid to transition from a very fine structure near locations of complex geometry such as film holes to a coarser structure far from the holes. Also note that the solid is not explicitly gridded, but the surface mesh completely defines the solid boundaries, and is thus sufficient to allow the BEM method to solve for the solid temperature field. An additional helpful feature of this grid is that all blocks have cell counts that are multiples of 4 to allow for two levels of multigrid flow computation. This feature allows for coarsening of the surface mesh in the BEM calculation as well.

CONVECTION CALCULATION METHOD

The calculation for the convective flow part of the problem was carried out using the multiblock flow solver Glenn-HT. This code was previously known as TRAF3D.MB [19], and is based on the single block code of Arnone et al. [20]. The code is a general purpose three-dimensional flow solver designed for computation of convective heat transfer of flows in complicated geometries. The code solves the full compressible Navier-Stokes equations using a multi-stage Runge-Kutta-based multigrid method. The finite volume method is used with central differencing, and artificial dissipation is employed. The overall accuracy of the code is second order. The present version of the code employs the k-ω turbulence model developed by Wilcox [21, 22], with modifications by Menter [23] as implemented by Chima [24]. Accurate heat transfer predictions are possible with the code because the model integrates to the walls and no wall functions are used. Rather, the computational grid is generated to be sufficiently fine near walls to produce a y^+ value of less than 1.0 at the first grid point away from the wall. A turbulent Prandtl number of 0.9 is used, and laminar viscosity is determined from temperature using a 0.7 power law [25]. Specific heats are assumed to be constant. A full description of the code and its recent applications to turbine heat transfer can be found in [26].

CONDUCTION CALCULATION METHOD

The Boundary Element Method (BEM) is used to solve the thermal conduction problem in the solid blade. Kassab et al. [16] describe this method in detail. A brief overview of the method is given here. As implemented in the present study, the three-dimensional Navier-Stokes flow solution is converged toward steady state by time marching. The three-dimensional steady heat conduction analysis is performed using BEM after every 100 iterations of the flow solver. This increment may be changed, but 100 time steps was found to be a good trade-off between convergence rate and CPU time, since each BEM step takes approximately 25 times as long as one flow solver time step. Moreover, the flow-solver uses an explicit scheme to advance the solution using local time-stepping and residual smoothing and as such produces solutions that are not physical, while the conduction solution is obtained by solving an elliptical problem at each iteration. Thus, it is better for the sake of convergence of the overall conjugate scheme not to iterate too often in the early stages as the solution evolves towards steady-state.

The governing equation for the steady conduction problem is:

$$\nabla \cdot [k_s(T_s)\nabla T_s] = 0 \qquad (1)$$

where T_s denotes the temperature of the solid and k_s is the solid thermal conductivity. For the present study, the thermal conductivity of the solid is taken to be a constant, so eqn. 1 reduces to the Laplace equation for temperature:

$$k_s \nabla^2 T_s = 0 \qquad (2)$$

Although not considered in the present study, cases with variable thermal conductivity may also be handled by converting the resultant nonlinear differential equation to a form of the Laplace equation using the Kirchhoff transform. For the conjugate analysis considered in this study, the problem remains linear in Kirchhoff transformed space as the boundary conditions at the fluid/solid interface also transform linearly.

The Laplace equation for thermal conduction is then converted into a boundary integral equation (BIE) as described in [27-29], which can be solved using the boundary surface discretization available from the convective grid. Although this grid physically lies only at the surface, the solution of the BIE contains information that can be used to determine the temperature at any point inside the solid volume as well. Typically, however, we are most concerned with thermal characteristics at the surface, and this is where the extreme values of temperature occur for solids without internal heat sources. It should be noted that although it was not implemented for the present work, the capability exists for extension of the BEM method to thermal stress analysis.

The BEM is implemented using an iterative domain decomposition approach whereby the surface grid is decomposed into a number of sub-domains with continuity of

heat flux and temperatures imposed at the sub-domain interfaces during the iteration process. A physically-based initial guess is used to impose the initial temperatures at the domain interfaces, a lower order BEM constant element model is then solved iteratively to convergence in order to provide the initial guess to a higher order bilinear BEM model. The process is readily implemented in parallel under MPI on a PC cluster with sub-domain optimally assigned to given processors on the cluster by a load balancing routine. The 85,000 DOF conduction problem arising from the current film-cooled blade model is decomposed into 20 sub-domains as shown in Figure 4. A stand-alone conduction problem may be solved to convergence on a PC cluster consisting of 10 Pentium IV PC's each with 1 GB SDRAM connected through a 100 base-T Ethernet network in nearly 50 minutes.

BOUNDARY CONDITIONS AND COUPLING

As shown in Figure 1, the freestream inlet flow to the vane is in the axial direction, with inlet stagnation properties set to engine operating conditions of 1726 K and 2574 kPa for temperature and pressure, respectively. The inlet turbulence intensity is 8 percent, and the length scale is 15 percent of true chord. Although the inlet flow conditions for this study are uniform, the effect of combustor exit non-uniformities on turbine vane thermal loads could be modeled through application of the appropriate inlet profiles. The freestream exit static pressure was set to a constant value of 1483 kPa. This value was determined empirically to yield the design exit Mach number of 0.876. Periodic boundary conditions were enforced in the tangential direction at the mid-pitch plane, and in the spanwise direction at either end of a single pitch of film cooling holes. The spanwise extent of the computational grid can be seen in Figure 3. The spanwise periodic assumption was enabled by the linear design of the vanes. Although a full-span calculation would better model variations due to coolant flow along the axis of the vane, this would have required gridding a domain approximately 17 times the spanwise extent, with a proportionate increase in cell count. Because of the spanwise periodic assumption, special treatment was required for the coolant inlet flow. In the actual geometry, the coolant flows axially along the plenum. However, this results in a coolant flow that is non-periodic as both the pressure and mass flow rate of the coolant decrease along the plenum axis. In order to maintain a truly spanwise periodic solution, the coolant was supplied to the plenum from the plenum wall opposite the holes. This is illustrated in Figure 1. The area over which the flow is supplied was chosen to be large enough to result in very low Mach numbers at these inlets (<0.05). The flows in the coolant supply cavities thus closely resemble true plena. This differs from the real case wherein the coolant is flowing along the axis of the plenum in the spanwise direction, and results in lower velocities in the plenum. This may have an effect on the conjugate calculations because the heat transfer coefficient inside the plenum may be underpredicted. The stagnation temperature of the coolant is set to 0.5 times the freestream inlet, or 863 K. The mass flow was set to the constant value required to give the design coolant flow rate over each plena's inflow patch.

The solid walls were given no-slip boundary conditions for velocity. The thermal boundary condition differed depending upon the type of calculation conducted. For the adiabatic solution, all solid walls were set to zero heat flux. Heat transfer coefficient and adiabatic wall temperature distributions for film cooling problems may be nondimensionalized by using Stanton number and film effectiveness, defined as:

$$St = q''/[(\rho V c_p)(T_{aw} - T_w)] \qquad (3)$$

and

$$\eta = (T_{in} - T_{aw})/(T_{in} - T_c) \qquad (4)$$

respectively.

For conjugate calculations, an iterative procedure was employed for setting the wall temperature and heat flux. First, the flow solver was run 100 iterations with an initial condition of adiabatic wall. Then the computed wall temperature distribution was sent to the conduction solver for a BEM solution of wall heat flux. This wall heat flux was then sent back to the flow solver and used as the thermal boundary condition for the next 100 iterations. This process was repeated until the entire coupled solution had converged, which typically required at least 3000 flow calculation iterations. Each BEM step required about 25 times as much time as a single flow time step. The 100/1 flow/BEM iteration ratio was found to give the best convergence rate per unit CPU time. The flow calculations were performed on a Cray SV1ex supercomputer, and required approximately 50 CPU hours to reach convergence.

The two cases for different values of solid thermal conductivity (Inconel and silicon nitride ceramic) will be presented. Inconel is a nickel-chromium-iron alloy known for its high strength and high temperature capability, and it is commonly used for turbine blades and vanes. The value of thermal conductivity for Inconel at the average vane temperature of 1208 K is 27.7 W/mK. The ceramic used for the comparison calculation is silicon nitride, with a thermal conductivity at the same average vane temperature of 8.0 W/mK. The thermal conductivity of both Inconel and silicon nitride are strongly dependent on temperature. The thermal conductivity of Inconel more than doubles from room temperature to 1208 K, while the value for silicon nitride nearly halves over the same range. The average vane temperature of 1208 K was determined as 70% of the inlet stagnation temperature, which is typical for a film-cooled vane with coolant at 50% of the inlet stagnation temperature. Future versions of the conjugate solver will be able to handle thermal conductivity

as a function of local temperature in addition to layers of materials, such as might be found with thermal barrier coatings (TBCs) and environmental barrier coatings (EBCs).

RESULTS

The overall flow physics of the problem will be shown in the next several figures, and is based on the Inconel vane solution. Figure 5 shows the stagnation temperature on a blade-to-blade plane through several of the film cooling holes. The temperatures are normalized by the freestream inlet stagnation temperature. Since the holes in the leading edge region are spanwise-angled, they are cut in several places by the coordinate plane. It can be seen that the shaped holes on the pressure side do a better job than the round holes on the suction side of laying down a layer of cold fluid close to the wall. Also, the stagnation point of the flow is illustrated by the location at which the hot freestream fluid approaches the vane between rows 6 and 7 in the showerhead region. Generally, coolant from rows 5 and 6 flows to the pressure side, while coolant from rows 7-10 flows to the suction side, leaving the gap between rows 6 and 7 uncovered. The thermal boundary layer is thicker on the pressure side due to the lower freestream velocities.

Figures 6 and 7 show the velocity vectors for a typical round and shaped hole, respectively. Vectors are shown for a uniform array of points, not at actual grid points. As indicated by Figure 5, the shaped hole effectively diffuses the coolant flow, keeping it near the vane surface where it can be effective. In contrast, the round holes exhibit a higher velocity at their exit plane, and are more susceptible to jet separation and liftoff. A common occurrence in round holes is the separation bubble downstream of the sharp inlet corner to the hole. This is caused by the rapid acceleration of the coolant around this sharp corner. The flow cannot remain attached, resulting in a recirculation zone. For low-to-moderate length-to-diameter ratio holes, this can adversely affect the film cooling performance, because the flow may not reattach before the flow exits the hole.

Figures 8, 9 and 10 show the vane surface temperature prediction for adiabatic wall, conjugate heat transfer with silicon nitride vane, and conjugate heat transfer with Inconel vane, respectively. The qualitative distributions for the three cases are quite similar. The temperature distributions show that the peak temperature occurs at the stagnation point between rows 6 and 7 for all cases. Figure 11 shows the span-averaged outer wall temperatures for the three cases, while Figure 12 presents the changes in span-averaged wall temperature between the conjugate cases and the adiabatic case. These two plots show that the peak stagnation point temperature is reduced as the thermal conductivity of the vane is increased. For the Inconel vane, the reduction is about $0.02T_{o,in}$, which corresponds to a 35 K reduction in temperature compared to the adiabatic wall prediction.

It can be seen in Figures 11 and 12 that the adiabatic wall case has the highest outer surface temperature over almost the entire vane, while the conjugate cases are closer to each other in temperature than to the adiabatic case. The lower outer wall temperatures for the conjugate cases are due to thermal conduction across the thickness of the vane wall from the outer surface to the inner (plenum) surface. However, an interesting counter example to this is evident on the pressure side of the vane near the first two rows of shaped holes, rows 3 and 4. Here, the Inconel case actually has a higher temperature than the adiabatic case. This is shown most clearly in Figure 12. One would expect the conjugate cases to always have a lower outer wall temperature based on one-dimensional thermal conduction in the solid from a hotter outer surface to a cooler plenum surface. The phenomenon may be understood by studying the heat flux distributions for the two conjugate cases, as shown in Figures 13, 14 and 15. Figures 13 and 14 suggest that the heat flux distribution for the two conjugate cases is similar, with the Inconel case having larger values because of the higher thermal conductivity (note the different scales in the two figures). This is confirmed by Figure 15, which presents the span-averaged values. The direction of heat flow at the surface (into the vane or into the fluid) is generally the same for the two conjugate calculations. The magnitude is reduced for the lower thermal conductivity case, as expected. Figure 15 also shows that the heat flux is into the solid for both cases in the showerhead and on the suction side of the vane, while the heat flux changes direction on the pressure side, but is primarily into the fluid. This behavior occurs because a film cooled vane is an example of a two-temperature mixing problem. As the coolant is injected at the surface of the vane, regions of heat flux into the fluid result where the wall temperature is higher than the adiabatic wall temperature. In these regions, one of which can be seen near rows 3 and 4 in Figures 13 and 14, the higher thermal conductivity of Inconel actually causes the wall temperature to increase. In general, the conjugate conduction reduces wall temperatures where heat flux is into the wall and increases them where heat flux is into the fluid. This behavior also indicates that the thermal conduction is not simply one-dimensional, but heat travels along the vane wall toward low temperature regions, such as near rows 3 and 4, from the hotter adjacent regions. These results show that it is too simplistic to assume that increasing vane conductivity will monotonically drive all surface temperatures toward the vane mean temperature, especially for a two temperature mixing problem such as turbine film cooling. Of course in the limit as the thermal conductivity increases to infinity, the vane would ultimately approach a uniform temperature.

Much of the preceding discussion hinges on the fact that the adiabatic wall effectiveness values presented in Figure 11 are quite high. This allows the direction of heat flow to be into the fluid over a large portion of the outer vane surface.

Although these values are in agreement with prior computational efforts for this geometry and similar film-cooled turbine vane cases (Heidmann, et al. [17] and Garg and Gaugler [30], respectively), the paucity of open literature film effectiveness data for such geometries makes definitive validation difficult. A future experimental study at NASA Glenn Research Center will provide much-needed film effectiveness data to corroborate this and other computational studies of realistic film-cooled turbine geometries.

Another interesting feature of the heat flux distributions in Figures 13 and 14 is the high heat flux into the fluid on the inside of the film cooling holes in rows 5-11, on the side of the hole nearest the outer wall. This is due to the proximity of this spot to the hot outer wall surface, and the high fluid velocities on that surface of the hole. The coolant accelerates around the sharp turn at the entrance of the film cooling hole and impinges on the opposite side as shown in Figure 6. This results in a high heat transfer coefficient. Heat is supplied to these spots by thermal conduction from the hot outer surface, which is very close in linear distance. If the showerhead and suction side holes in rows 5-11 could be redesigned to increase this impingement, perhaps the outer wall temperatures in this region could be reduced further. This would be especially important in the stagnation region where the peak temperatures occur.

SUMMARY AND CONCLUSIONS

Convective heat transfer calculations have been performed for the Honeywell film cooled vane geometry using the Glenn-HT code with coupled Boundary Element Method solution of conductive heat transfer in the vane. The Boundary Element Method does not require discretization of the solid volume. Only a surface grid is required, which already exists for the flow calculation. An adiabatic wall flow solution is presented for comparison.

Although the incorporation of conjugate heat transfer does result in the expected smoothing of the vane surface temperature with increasing thermal conductivity, there are secondary heat transfer effects. These effects result from the fact that wall heat flux values are not always into the solid on the outer surface of the vane, because film cooling is a two-temperature problem. The resultant redistribution of heat in the vane solid is made possible by three-dimensional thermal conduction. Heat travels along the vane wall, not simply one-dimensionally from outer surface to plenum surface. The heat flux at the wall for the two conjugate cases changes direction over the blade outer surface. It is into the fluid at some locations and into the solid at others. The direction is generally the same for both cases at a given location, but the magnitude scales with the solid thermal conductivity. High heat flux is seen on the impingement side of the round film cooling holes.

Future work in this project will consist of implementing variable thermal conductivity capability into the BEM solver. This is especially important for the large temperature range problems of interest in cooled turbines. The thermal conductivities of both metallic and ceramic materials can have a strong dependence on temperature. Layered material capability is another area for future development, as this will find application to TBC- and EBC-coated vanes and blades. Finally, thermal stress computation will be enabled by a similar BEM method.

REFERENCES

[1] Kays and Crawford, 1980, *Convective Heat and Mass Transfer*, 2nd ed., McGraw-Hill, New York, pp. 217.

[2] Bohn, D., Bonhoff, B., Schonenborn, H., and Wilhelmi, H., 1995, "Validation of a Numerical Model for the Coupled Simulation of Fluid Flow and Diabatic Walls with Application to Film-Cooled Gas Turbine Blades", VDI-Berichte Nr. 1186.

[3] Bohn, D., Bonhoff, B., Schonenborn, H., and Wilhelmi, H., 1995, "Prediction of the Film-Cooling Effectiveness of Gas Turbine Blades Using a Numerical Model for the Coupled Simulation of Fluid Flow and Diabatic Walls", AIAA Paper 95-7105.

[4] Bohn, D., Bonhoff, B., and Schonenborn, H., 1995, "Combined Aerodynamic and Thermal Analysis of a Turbine Nozzle Guide Vane", IGTC-paper-108, Proc. of the 1995 Yokohama Int. Gas Turbine Congress.

[5] Bohn, D., Becker, V., Kusterer, K., Otsuki, Y., Sugimoto, T., and Tanaka, R., 1999, "3-D Internal Flow and Conjugate Calculations of a Convective Cooled Turbine Blade with Serpentine-Shaped and Ribbed Channels", ASME Paper 99-GT-220.

[6] Takahashi, T., Watanabe, K., and Takahashi, T., 2000, "Thermal Conjugate Analysis of a First Stage Blade in a Gas Turbine", ASME Paper 2000-GT-251.

[7] Han, Z.-X., Dennis, B. H., and Dulikravich, G. S., 2000, "Simultaneous Prediction of External Flow-Field and Temperature in Internally Cooled 3-D Turbine Blade Material", ASME Paper 2000-GT-253.

[8] Rigby, D. L. and Lepicovsky, J., 2001, "Conjugate Heat Transfer Analysis of Internally Cooled Configurations", ASME Paper 2001-GT-405.

[9] Montenay, A., Pate, L., and Duboue, J. M., 2000, "Conjugate Heat Transfer Analysis of an Engine Internal Cavity", ASME Paper 2000-GT-282.

[10] Verdicchio, J. A., Chew, J. W., and Hills, N. J., 2001, "Coupled Fluid/Solid Heat Transfer Computation for Turbine Discs", ASME Paper 2001-GT-0205.

[11] Okita, Y. and Yamawaki, S., 2002, "Conjugate Heat Transfer Analysis of Turbine Rotor-Stator System", ASME Paper GT-2002-30615.

[12] Luff, J. K. and McGuirk, J. J., 2001, "Numerical Prediction of Combustor Heatshield Flow and Heat Transfer with Sub-Grid-Scale Modelling of Pedestals", ASME Paper 2001-GT-0144.

[13] Li, H. J. and Kassab, A. J., 1994, "Numerical Prediction of Fluid Flow and Heat Transfer in Turbine Blades with Internal Cooling", AIAA/ASME Paper 94-2933.

[14] Li, H. J. and Kassab, A. J., 1994, "A Coupled FVM/BEM Solution to Conjugate Heat Transfer in Turbine Blades", AIAA Paper 94-1981.

[15] Ye, R., Kassab, A. J., and Li, H. J., 1998, FVM/BEM Approach for the Solution of Nonlinear Conjugate Heat Transfer Problems, *Proc. BEM 20*, Kassab, A. J., Brebbia, C. A., and Chopra, M. B., (eds.), Orlando, Florida, August 19-21, 1998, pp. 679-689.

[16] Kassab, A. J., Divo, E., Heidmann, J. D., Steinthorsson, E., and Rodriguez, F., "BEM/FVM Conjugate Heat Transfer Analysis of a Three-Dimensional Film Cooled Turbine Blade", International Journal for Numerical Methods in Heat Transfer and Fluid Flow, (in press).

[17] Heidmann, J. D., Rigby, D. L., and Ameri, A. A., 2000, "A Three-Dimensional Coupled Internal/External Simulation of a Film-Cooled Turbine Vane", ASME Journal of Turbomachinery, Vol. 122, pp. 348-359.

[18] Program Development Corporation, 1997, "GridPro™/az3000 User's Guide and Reference Manual", White Plains, NY.

[19] Steinthorsson, E., Liou, M.-S., and Povinelli, L. A., 1993, "Development of an Explicit Multiblock/Multigrid Flow Solver for Viscous Flows in Complex Geometries", AIAA Paper 93-2380.

[20] Arnone, A., Liou, M.-S., and Povinelli, L. A., 1991, "Multigrid Calculation of Three-Dimensional Viscous Cascade Flows", AIA Paper 91-3238.

[21] Wilcox, D. C., 1994, *Turbulence Modeling for CFD*, DCW Industries, Inc., LaCanada, CA.

[22] Wilcox, D. C., 1994, "Simulation of Transition with a Two-Equation Turbulence Model", AIAA Journal, Vol. 32, No. 2, pp. 247-255.

[23] Menter, F. R., 1993, "Zonal Two-Equation k-ω Turbulence Models for Aerodynamic Flows", AIAA Paper 93-2906.

[24] Chima, R. V., 1996, "A k-ω Turbulence Model for Quasi-Three-Dimensional Turbomachinery Flows", NASA TM-107051.

[25] Schlichting, H., 1979, *Boundary Layer Theory*, 7th ed., McGraw-Hill, New York, pp. 312-313.

[26] Garg, V. K., 2002, "Heat Transfer Research on Gas Turbine Airfoils at NASA GRC", Int. J. of Heat and Fluid Flow, Vol. 23, pp. 109-136.

[27] Brebbia, C. A., Telles, J. C. F., and Wrobel, L. C., 1984, *Boundary Element Techniques*, Springer-Verlag, Berlin.

[28] Brebbia, C. A. and Dominguez, J., 1989, *Boundary Elements: An Introductory Course*, Computational Mechanics Pub., Southampton and McGraw-Hill, New York.

[29] Banerjee, P. K., 1994, *Boundary Element Method*, McGraw-Hill, New York.

[30] Garg, V. K and Gaugler, R. E., 1995, "Leading Edge Film Cooling Effects on Turbine Blade Heat Transfer", ASME Paper 95-GT-275.

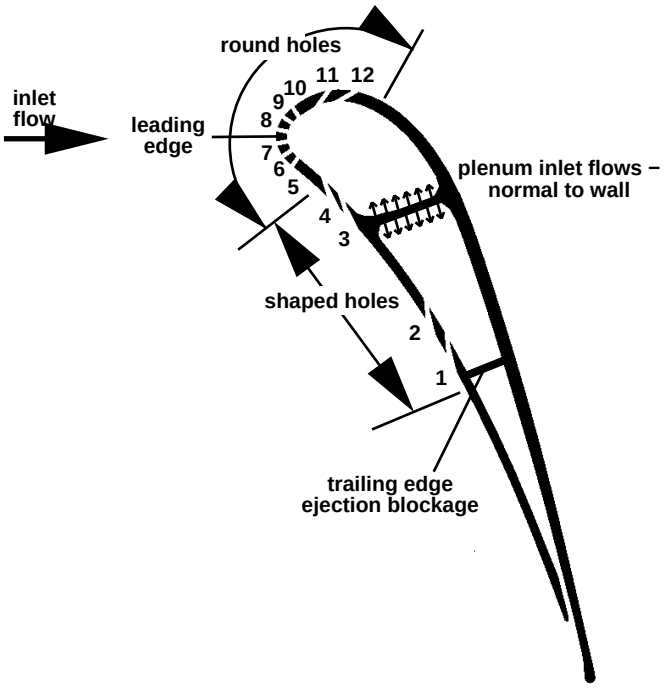

Figure 1: Vane cross−section and film hole row numbers

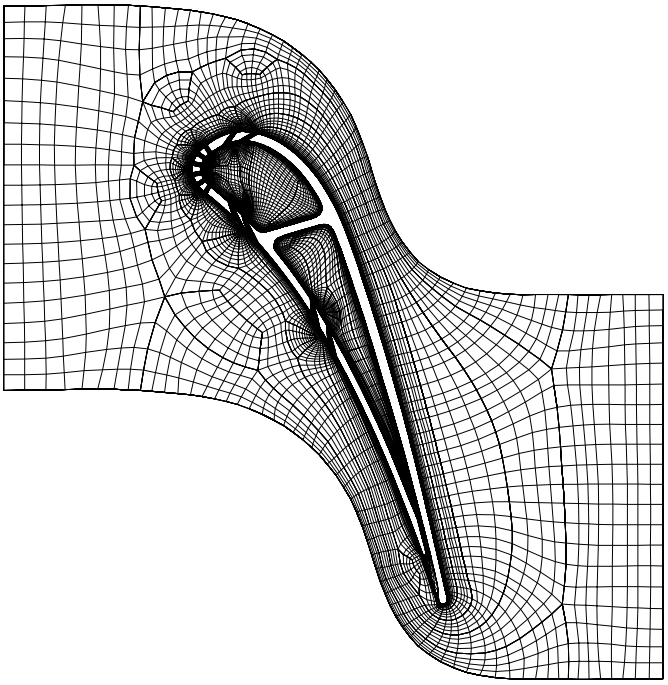

Figure 2: Blade−to−blade view of multiblock computational grid

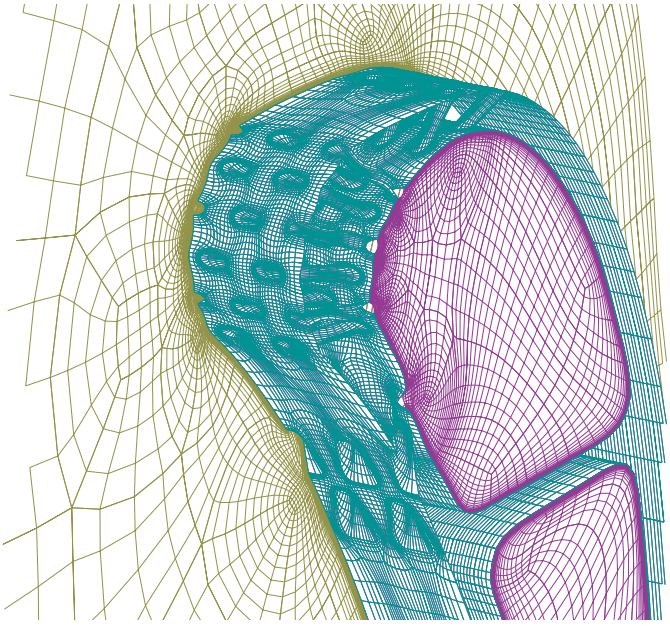

Figure 3: Leading edge region of computational grid

Figure 4: BEM domain decomposition for vane

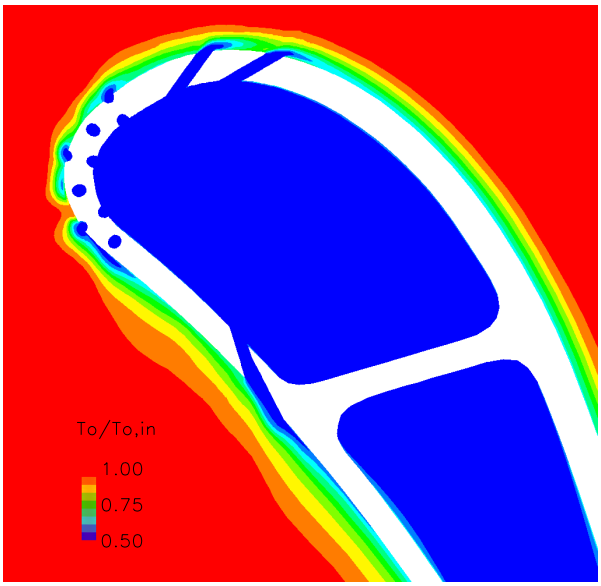

Figure 5: Stagnation temperature on cross−sectional plane with Inconel vane material

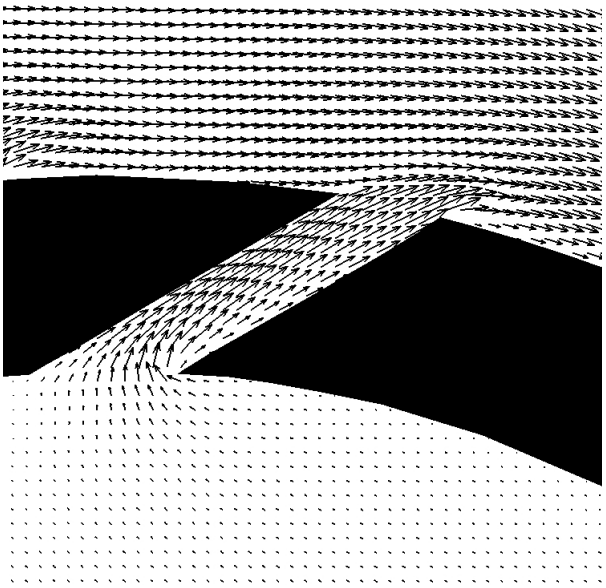

Figure 6: Velocity vectors on centerline of hole in row 12 (round)

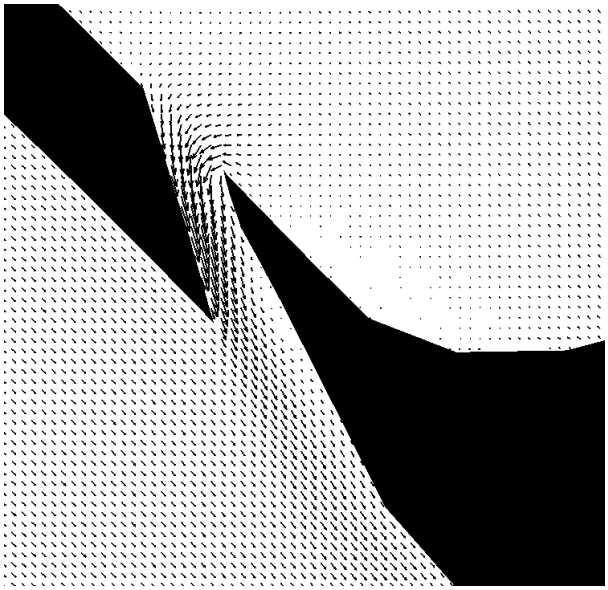

Figure 7: Velocity vectors on centerline of hole in row 3 (shaped)

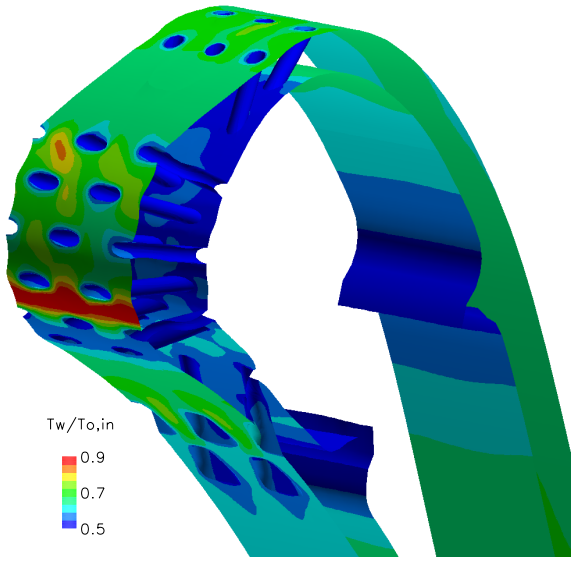

Figure 8: Wall temperatures for adiabatic wall case

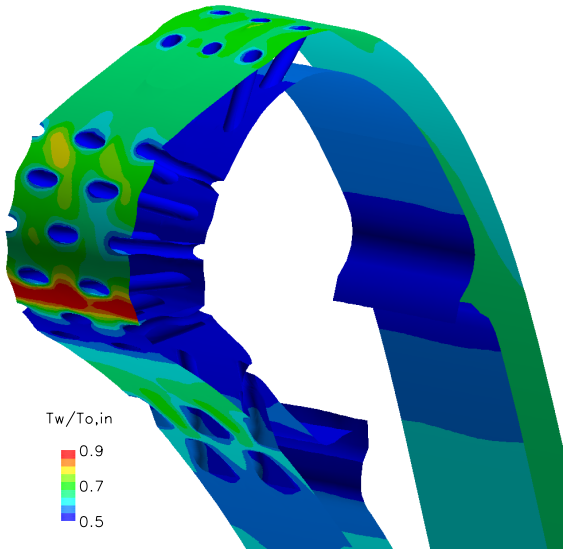

Figure 9: Wall temperatures for silicon nitride vane case

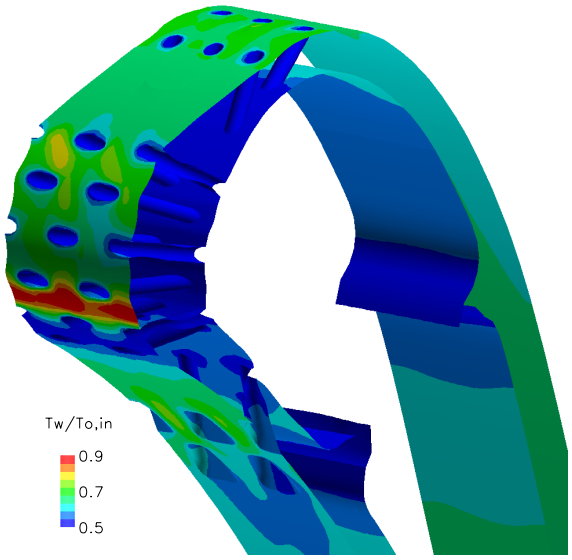

Figure 10: Wall temperatures for Inconel vane case

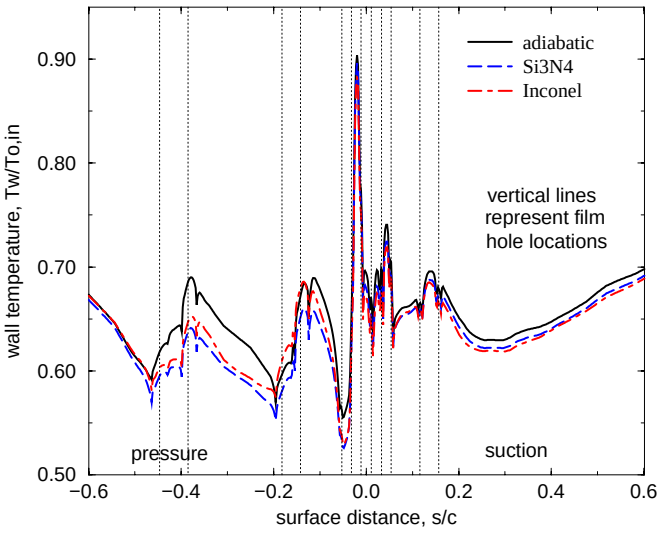

Figure 11: Span−averaged vane outer surface temperature

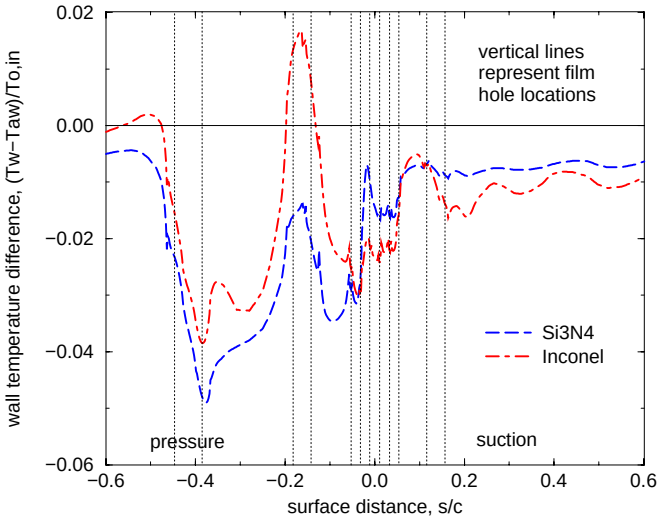

Figure 12: Span−averaged vane outer surface temperature difference

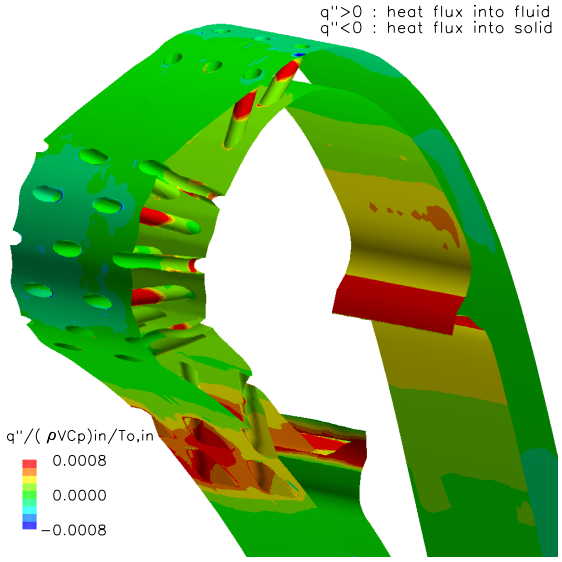

Figure 13: Wall heat flux for silicon nitride vane case

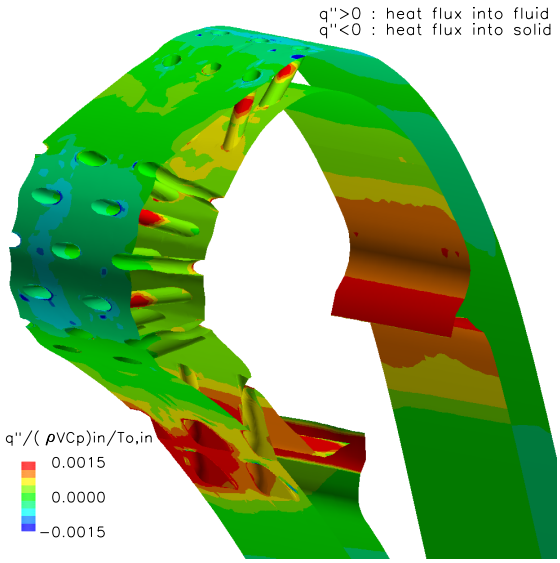

Figure 14: Wall heat flux for Inconel vane case

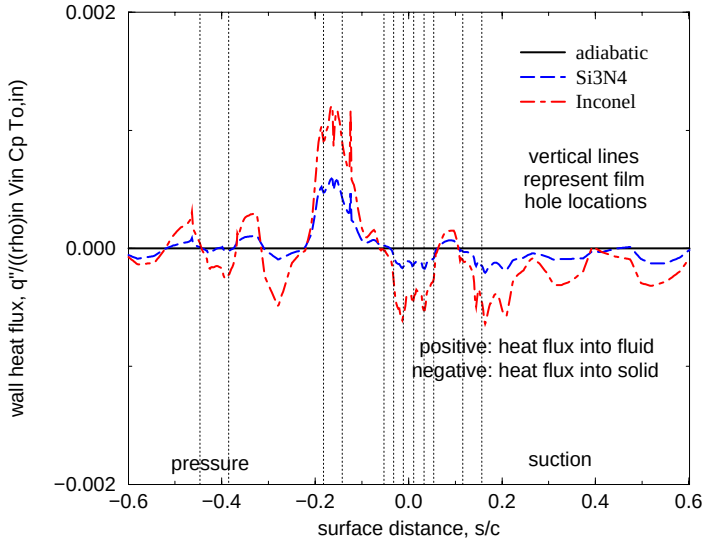

Figure 15: Span−averaged vane outer surface heat flux